Electrothermal filamentation of igniting plasmas

H. Martin,[1] R. W. Paddock,[1] M. W. von der Leyen,[1] V. Eliseev,[1,2,3] R. T. Ruskov,[1] R. Timmis,[1] J. J. Lee,[1] A. James,[1] and P. A. Norreys[1,4]

[1]*Department of Physics, Atomic and Laser Physics sub-department, Clarendon Laboratory, University of Oxford, Parks Road, Oxford OX1 3PU, United Kingdom*

[2]*IBM Research Europe, The Hartree Centre, Daresbury Laboratory, Keckwick Lane, Warrington WA4 4AD, United Kingdom*

[3]*Wrexham University, Mold Rd, Wrexham LL11 2AW, United Kingdom*

[4]*John Adams Institute for Accelerator Science, Denys Wilkinson Building, University of Oxford, Keble Road OX1 3RH, United Kingdom*

(Received 17 January 2024; accepted 29 July 2024; published 12 September 2024)

Dense, hot plasmas are susceptible to the electrothermal instability: a collisional process which permits temperature perturbations in electron currents to grow. It is shown here that linearizing a system comprised of two opposing currents and a mobile ion background as three distinct fluids yields unstable modes with rapid growth rates ($\sim 10^{13}$ s^{-1}) for wavenumbers below a threshold k_{th}. An analytical threshold condition is derived, this being surpassed for typical hot-spot and shell parameters. Particle-in-cell simulations successfully benchmark the predicted growth rates and threshold behavior. Electrothermal filamentation within the shell will impact the burn wave propagation into the cold fuel and resulting burn dynamics.

DOI: 10.1103/PhysRevE.110.035205

I. INTRODUCTION

Electron currents within collisional plasmas are susceptible to the electrothermal instability (ETI), a mechanism which permits temperature perturbations within currents to grow [1]. Intuitively, the ETI can be understood by considering a small perturbation in the temperature along a direction perpendicular to the current. Regions with higher temperature exhibit an enhanced electrical conductivity, driving an increase in the current density. These temperature peaks then experience a larger Ohmic heating rate, meaning the electron temperature increases faster than in the corresponding troughs. Via this feedback, hot regions become hotter, and perturbations grow.

This Letter addresses the impact of this phenomenon within the dense DT shell layer of an imploded inertial confinement fusion (ICF) target for the first time. Numerical simulations predict the shell to be characterized by densities of $n \sim 10^{32}$ m^{-3} and temperatures of $T \sim 0.5$ keV [2]. Under such extreme densities the plasma is strongly collisional; for the parameters above, the electron-ion collision time is $\tau_{\mathrm{ei}} \sim 0.02$ fs, and so effects such as the ETI which are mediated by collisions may develop very rapidly. In the central hot-spot ignition scheme for ICF, the kinetic energy of the implosion is converted to form a lower density ($n \sim 10^{31}$ m^{-3}), higher temperature ($T \sim 5$ keV) plasma, surrounded by the thin, dense fuel shell described above. The capsule comes to rest for about 0.1 ns, during which DT fusion reactions begin within the hotspot. A portion of the most energetic hot-spot electrons will stream outwards into the surrounding shell. This hot electron current drives a cooler, dense return current within the shell. Residual spherical asymmetries associated with the radiation drive and hydrodynamic instabilities will seed temperature perturbations in the return current, which will grow via the mechanism outlined here (see Fig. 1).

The ETI is a well understood problem in the context of conducting solids, often seen as a seed for the magneto–Rayleigh-Taylor instability which inhibits the implosion of metal cylinders in magnetic confinement fusion experiments [3,4]. Less literature is dedicated to the instability in plasmas, particularly those relevant to conventional inertial fusion, and could have a material impact on the performance of laser driven fusion capsules. Haines [1] first investigated the ETI in the corona of laser-produced plasmas, and since, much evidence has been put forth documenting filamentation consistent with this instability [5–11]. Treating the cold return current as a fluid under the MHD approximation, Haines derives a maximum growth rate for the instability

$$\gamma \approx 2\frac{m_{\mathrm{e}}}{m_{\mathrm{i}}}\nu_{\mathrm{ei}}, \tag{1}$$

where ν_{ei} is the electron-ion collision frequency, and m_{e}, m_{i} are the electron and ion masses, respectively.

This approximation is now relaxed in this work, permitting the cold electron and ion fluids to separate. The similar collisional Weibel instability has been studied, but treatments assume a uniform temperature [12,13]. The well-known heat-flux instabilities of [14,15] apply to the ablating target plasma, but not to the condensed shell considered here.

II. LINEAR THEORY

Throughout this work, the hot electron current, cold return current, and background ions are treated as three separate fluids. Their behavior is determined by conservation of mass, momentum, and internal energy, respectively,

$$\frac{\partial n_j}{\partial t} + \nabla \cdot (n_j \mathbf{v}_j) = 0, \tag{2}$$

$$m_j n_j \left(\frac{\partial}{\partial t} + \mathbf{v}_j \cdot \nabla \right) \mathbf{v}_j = -\nabla p_j - \nabla \cdot \pi_j + n_j q_j (\mathbf{E} + \mathbf{v}_j \times \mathbf{B}) + \mathbf{R}_j, \tag{3}$$

$$\frac{3}{2} n_j \left(\frac{\partial}{\partial t} + \mathbf{v}_j \cdot \nabla \right) T_j = -n_j T_j \nabla \cdot \mathbf{v}_j + \pi_j \cdot \nabla \mathbf{v}_j + \nabla \cdot \mathbf{q}_j + Q_j, \tag{4}$$

where $j = \mathrm{c, h, i}$ denote the cold, hot, and ion species respectively. p_j and π_j are the pressure scalars and tensors, $\mathbf{R}_j$ is the friction force due to collisions, Q_j is the heat generated by collisions, and $\mathbf{q}_j$ is the heat flux, each for species j. Note, Boltzmann's constant is omitted throughout this Letter. This system of equations is closed by choosing the Braginskii transport coefficients, permitting the various unknown moments to be expressed in terms of $n_j, \mathbf{v}_j$, and T_j [16]. The dynamics of the electromagnetic fields generated are captured entirely by Faraday's and Ampère's laws,

$$\frac{\partial \mathbf{B}}{\partial t} = -\nabla \times \mathbf{E}, \tag{5}$$

$$\mu_0 \epsilon_0 \frac{\partial \mathbf{E}}{\partial t} = \nabla \times \mathbf{B} - \mu_0 (\mathbf{J}_\mathrm{c} + \mathbf{J}_\mathrm{h} + \mathbf{J}_\mathrm{i}). \tag{6}$$

The use of a fluid description to model this system deserves comment. Whilst the transport of the hot electrons from the hotspot to the surrounding cold fuel is strictly a kinetic problem, the subsequent instability growth is well described by hydrodynamics. This is owing to the rapid collision frequency between cold electrons, and between ions within the dense fuel plasma, where such collisions restrict the local particle distribution functions to be closely Maxwellian. This does not hold for the effectively collisionless hot electrons, which are assumed to couple to the cold plasma species only via collective fields. The hot electron current is modeled as a beam with a constant transverse temperature T_h and an initial velocity of $v_{\mathrm{h}y} = -0.3c$, reflecting the fact that the hot electrons have a velocity $\sim$2–3 times the thermal velocity [1] of the hotspot with temperature $T_\mathrm{h} = 5$ keV. The hot electron temperature is taken to be constant on the basis that the hot electron collision time is $\sim$6 orders of magnitude larger than the cold electrons (assuming $n_\mathrm{h}/n_\mathrm{c} = 0.01$), thus Eq. (4) is omitted for the hot electrons.

Before considering the dynamics of perturbations, attention should first be given to the behavior of the unperturbed background system. It is supposed that initially the hot and cold currents stream antiparallel along the y axis, and are of equal magnitude such that

$$\mathbf{J}_\mathrm{c} + \mathbf{J}_\mathrm{h} = 0. \tag{7}$$

A uniform electric field $\mathbf{E} = E_y \hat{\mathbf{y}}$ exists along the same axis as the electron currents, as drawn in Fig. 1. This field arises due

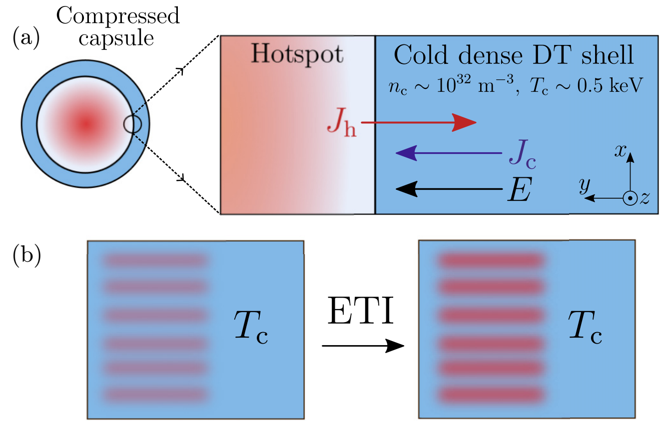

FIG. 1. Schematic detailing the geometry of the system considered, with (a) the propagation of the hot electron current into the cold shell and (b) the growth of temperature filaments in the cold return current via the ETI.

to an electrostatic charge separation produced by the motion of the hot electron current, and acts to accelerate the cold electrons in the opposite direction. Both sets of currents are imposed on a background of mobile ions, taking $Z = 1$ for a hydrogen plasma.

The cold electron current is collisional and so experiences a friction force that opposes the acceleration due to $\mathbf{E}$. Initially these forces are balanced, allowing the appropriate initial electric field strength to be found. In the absence of time or spatial derivatives, and writing the friction force as $\mathbf{R}_\mathrm{c} = e n_\mathrm{c} \mathbf{J}_\mathrm{c}/\sigma_\mathrm{c}$, Eq. (3) reduces to Ohm's law

$$\mathbf{E}_0 = \frac{\mathbf{J}_{0\mathrm{c}}}{\sigma_{0\mathrm{c}}}, \tag{8}$$

where σ_{0c} is the cold electron conductivity, and the subscript "0" indicates an unperturbed background quantity at some initially defined time. This distinction is necessary as the background system described here is inherently time dependent, which a realistic treatment cannot neglect. Taking $\nabla \to 0$ in Eqs. (2)–(6) to reflect the absence of perturbations, the background system is described by the following coupled equations:

$$n_\mathrm{c} \frac{\partial v_{\mathrm{c}y}}{\partial t} = -n_\mathrm{c} e E_y - 0.51 \frac{n_\mathrm{c}}{\tau_\mathrm{c}} v_{\mathrm{c}y}, \tag{9}$$

$$n_\mathrm{h} \frac{\partial v_{\mathrm{h}y}}{\partial t} = -n_\mathrm{h} e E_y, \tag{10}$$

$$\frac{3}{2} n_\mathrm{c} \frac{\partial T_\mathrm{c}}{\partial t} = n_\mathrm{c} \frac{v_\mathrm{c}^2}{\tau_\mathrm{c}} - \frac{3 m_\mathrm{e}}{m_\mathrm{i}} \frac{n_\mathrm{c}}{\tau_\mathrm{c}} (T_\mathrm{c} - T_\mathrm{i}), \tag{11}$$

$$\frac{3}{2} n_\mathrm{i} \frac{\partial T_\mathrm{i}}{\partial t} = \frac{3 m_\mathrm{e}}{m_\mathrm{i}} \frac{n_\mathrm{c}}{\tau_\mathrm{c}} (T_\mathrm{c} - T_\mathrm{i}), \tag{12}$$

$$\epsilon_0 \frac{\partial E_y}{\partial t} = e n_\mathrm{h} v_{\mathrm{h}y} + e n_\mathrm{c} v_{\mathrm{c}y}, \tag{13}$$

where ion motion is neglected for the sake of the background analysis. Equations (9)–(13) form a coupled nonlinear system, and can be readily understood qualitatively. The cold electron fluid is heated through collisions with the background ions, with this increased temperature reducing the frictional force on the electrons. The initial balance of this friction and E_y is lost, the cold electron fluid begins to accelerate, and the resulting net current couples to the external electric field E_y via Ampère's law, leading to damped oscillations and a net shift in E_y, v_{cy}, and v_{hy}. A straightforward approach is to neglect this background behavior and simply proceed using the initial value of each background quantity to carry out the linearization of Eqs. (2)–(6). This was found to overestimate the growth rate by an order of magnitude, largely due to neglecting the significant reduction of the driving field E_y. This error is avoided by time averaging the numerical solution of Eqs. (9)–(13). This time averaging is self consistent if carried out over a duration $\tau_{av} \sim \gamma^{-1}$, where γ is the resulting growth rate predicted by the dispersion relation. *A priori*, the growth rate is not known, so time averaging is carried out over the scale given by Eq. (16) in the following analysis.

A first estimate of the electrothermal growth rate can be made by considering two timescales inherent to the instability. Neglecting the effect of any self-generated fields, the instability is mediated via electron-ion collisions and the acceleration of cold electrons via the external field. These processes are reflected in the cold electron-ion collision time τ_c and

$$\tau_E = \frac{\sqrt{m_e T_c}}{eE_y}, \tag{14}$$

respectively. By supposing small perturbations to the cold electron conservation equations in the long wavelength limit where gradient terms vanish, and assuming (8) is always satisfied, it can be shown analytically that perturbations grow as

$$\delta T_c \propto e^{t/\tau_\Omega}, \tag{15}$$

introducing the electrothermal timescale

$$\tau_\Omega = \frac{\tau_E^2}{\tau_c}. \tag{16}$$

Adopting $n_c = 10^{32}$ m^{-3}, $T_c = 0.5$ keV, and assuming a hot-cold ratio of $n_h/n_c = 0.01$ yields $\tau_\Omega \sim 8$ fs. This timescale is particularly sensitive to the hot electron current density, with Eqs. (7), (8), and (14) implying $\tau_\Omega \propto (n_h/n_c)^{-2}$. This is in contrast to Eq. (1) which is independent of the hot current.

A dispersion relation is now derived for 1D perturbations to the background system described. Perturbations along $\hat{\mathbf{x}}$ are considered, perpendicular to both currents. There are a total of 14 amplitudes relevant to this problem, which, for clarity, are n_j, v_{jx}, v_{jy}, T_j for both cold electrons and ions, n_h, v_{hx}, v_{hy} for the hot electrons, and the fields E_x, E_y, B_z. Note E_x and B_z are purely self-generated. Supposing perturbations of the form $\delta \propto \exp i(kx - \omega t)$, Eqs. (2)–(6) reduce to a 14-dimensional linear system of the form $M(k,\omega)\mathbf{x} = \mathbf{0}$. The solutions to the corresponding characteristic equation $\mathrm{Det}(M) = 0$ cannot be found via analytical methods for such a large system, so numerical dispersion curves are obtained for a range of cold electron temperatures. These curves are plotted in Fig. 2, demonstrating the existence of unstable modes with growth rates on the order of 10^{13} s^{-1} below a cutoff wave vector. For long wavelengths where self-generated fields are negligible, the limit $\mathrm{Im}(\omega) \to \langle \tau_\Omega^{-1} \rangle$ is approximately recovered, where $\langle \cdot \rangle$ indicates a time average. As k increases, self-generated

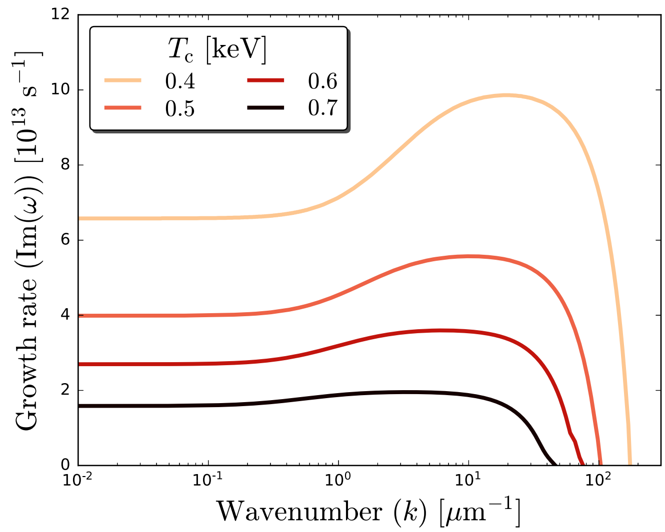

FIG. 2. Numerical dispersion curves giving the growth rate as a function of wavenumber k for a range of cold electron temperatures. The parameters $n_c = 10^{32}$ m^{-3}, $n_h/n_c = 0.01$, and $v_{hy} = -0.3c$ are assumed.

fields act to enhance the instability, where this effect is eventually curtailed by the cold electron thermal conductivity κ_c which acts to eliminate temperature variation in T_c at small wavelengths. Note that these modes are nonconvective, i.e., $\mathrm{Re}(\omega) = 0$.

An analytical threshold condition for the electrothermal instability exists, and is found by considering the characteristic equation when $\mathrm{Im}(\omega) = 0$. Defining k_{th} as the solution to $\mathrm{Im}(\omega(k)) = 0$, the equation $\mathrm{Det}(M(0, k_{th})) = 0$ reduces to a quadratic in k_{th}^2 with solution

$$k_{th}^2 = \frac{9}{2}\frac{|E_y|}{T_c\kappa_c}\left(J_h - \frac{1}{3}|E_y|\sigma_c - \frac{2n_c T_c}{3\tau_c}\frac{m_e}{m_i}\frac{1}{|E_y|}\right). \tag{17}$$

Requiring that $k_{th}^2 > 0$ ensures that k_{th} is real, and constitutes a necessary and sufficient condition for the existence of unstable modes. This requirement can be written as an explicit condition on the hot electron current via the above by recognizing that $J_h - 1/3|E_y|\sigma_c = 2/3J_h$, assuming Eqs. (7) and (8) are satisfied. We then require that

$$J_h^2 > \frac{n_c T_c}{\tau_c}\frac{m_e}{m_i}\sigma_c. \tag{18}$$

Using the Braginskii result for σ_c, this reduces to the form

$$J_h > \frac{7}{5}\sqrt{\frac{m_e}{m_i}}\sqrt{\frac{T_c}{m_e}}n_c e. \tag{19}$$

To demonstrate that this condition is readily satisfied for an ICF plasma, T_c can be written in terms of the cold electron thermal velocity $\tilde{v}_c$, yielding

$$v_h > v_{th} = \frac{7}{5\sqrt{3}}\sqrt{\frac{m_e}{m_i}}\frac{n_c}{n_h}\tilde{v}_c. \tag{20}$$

For a hot-cold ratio $n_h/n_c \sim 10^{-2}$, we find a threshold hot electron current velocity $v_{th} \approx 1.2\tilde{v}_c$. The hot current arises due to the high-energy tail in the distribution of hot-spot electrons, meaning this threshold is comfortably surpassed for the case of an imploded fusion target where typically the hotspot is an order of magnitude hotter than the surrounding shell [2]. Permitting this, modes with $k < k_{\mathrm{th}}$ are then unstable. Equation (20) describes a similar threshold to that predicted by [1]; Comparison of the threshold heat flux associated with (20) to the form derived in [1] yields $q_{\mathrm{th}}/q_{\mathrm{th}}^{\mathrm{H}} = 5/2 n_{\mathrm{h}} v_{\mathrm{th}}(T_{\mathrm{h}} - T_{\mathrm{c}})/q_{\mathrm{th}}^{\mathrm{H}} \approx 0.95$, independent of any parameters.

It is worth noting that the cold, dense plasma parameters involved here constitute a semi-ideal, semidegenerate plasma [17]. Accounting for both electron-ion coupling and degeneracy in this transition region is involved, and so, for simplicity, is neither accounted for in this analysis or by the PIC simulations to follow. Lee and More [18] provide degenerate corrections to the Braginskii transport coefficients, which evaluate to order of unity factors for the parameters used here. These corrections are only partially valid as their work assumes that Z is not small, being invalid for a hydrogen plasma. A more concrete justification for neglecting degenerative effects is offered by Lambert *et al.* [19], who evaluate the electrical and thermal conductivity for hydrogen over a broad parameter range via a quantum molecular dynamic approach. They report departures from the Braginskii/Spitzer transport coefficients by a factor $\lesssim 2$ for both conductivities assuming cold fuel shell parameters. These corrections will not change the growth rates obtained in Fig. 2 by a considerable amount, nor the threshold wavenumbers, and so the use of Braginskii transport coefficients is justified for this application.

III. PIC SIMULATIONS

The particle-in-cell code SMILEI [20] was employed to simulate the ETI over a broad range of wavelengths. Given this instability involves gradients along a single axis, one-dimensional simulations are sufficient. The simulations were initialized with balanced cold and hot currents, represented by two distinct macroparticle species. Two cases were considered for $T_{\mathrm{c}} = 0.5$ and 0.7 keV, with a hot electron temperature $T_{\mathrm{h}} = 10T_{\mathrm{c}}$ assumed in both. A third species was used to represent the mobile ion background with $T_{\mathrm{i}} = T_{\mathrm{c}}$. Densities of $n_{\mathrm{c}} = 10^{32}\ \mathrm{m}^{-3}$ and $n_{\mathrm{h}} = 0.01 n_{\mathrm{c}}$ were assumed, and a uniform electric field E_{0y} was placed along the current axis. The instability was seeded via an initial 10% perturbation in the cold electron temperature, where the amplitude of this perturbation was evaluated at each timestep allowing the growth rate to be measured. These simulated rates are plotted in Fig. 3, imposed on the dispersion relations predicted by our linear theory. The simulations document good agreement with linear theory, confirming modes are unstable for wavenumbers smaller than the predicted threshold k_{th}. The linear theory appears to generally overestimate the simulated positive growth rates, likely caused by the simulated average value of E_{0y} being slightly smaller than Eqs. (9)–(13) predict. For $k > k_{\mathrm{th}}$, temperature perturbations are found to decay as expected.

The shell Debye length was resolved using a grid spacing $\Delta x = \lambda_{\mathrm{D}}/2 \approx 8.3$ pm, with corresponding CFL condition satisfied using a timestep $\Delta t = 0.35\Delta x/c \approx 10^{-20}$ s. This restrictive timestep makes resolving entire e-foldings of the instability infeasible, and thus, these simulations capture only

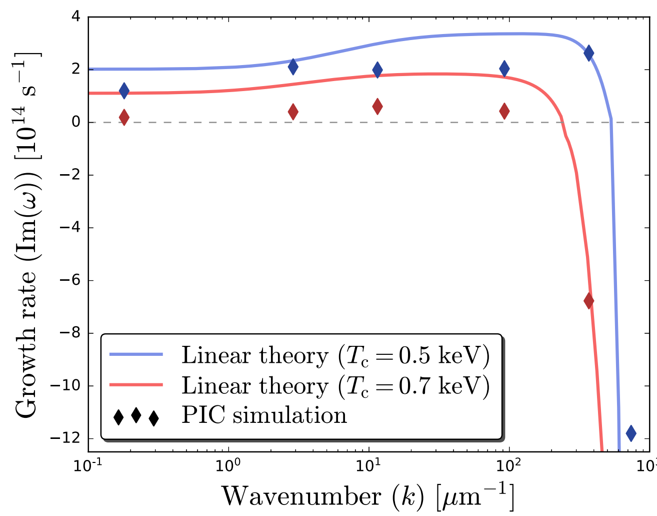

FIG. 3. Growth rates obtained from a series of 1D PIC simulations, benchmarked against the corresponding dispersion relation predicted by linear theory.

the initial linear growth over a time length of 4×10^{-17} s. Capturing emergent collisional phenomena such as Ohmic heating and thermal conduction via a PIC approach requires extremely good resolution, owing to the large number of macroparticles required to truthfully replicate these statistical processes. A few 10^8 macroparticles were used for the smaller wavenumbers, with a few 10^7 for larger ones. For each simulation, using fewer macroparticles was found to cause fluctuations in the cold electron temperature on the order of the initially seeded perturbation. SMILEI implements binary collisions following the algorithm proposed by Perez *et al.* [21]. Benchmarking demonstrates that this approach reproduces Spitzer-like conductivity in high temperature simulations but only to within an order unity constant [20]. Consequently, using a Spitzer/Braginskii form for σ_c in Eq. (8) will not provide the precise field strength E_{0y} necessary to initially balance the forces on the cold electron current. This imbalance was found to lead to unphysically large oscillations in E_y and J_{cy}. This was remedied by tuning the initial value of E_{0y} slightly until the initial acceleration of the cold electron fluid vanished. For a meaningful comparison, the value of E_{0y} and implied electron-ion collision time found by this process was used in producing the dispersion relation in Fig. 3. The simulated electron-ion collision times were found to be factors 0.65 and 0.62 smaller than the Braginskii results for the 0.5 keV and 0.7 keV cases, respectively. The averaging of the background system was carried out over the simulation time length, resulting in the increased growth rates given by the curves in Fig. 3 compared to Fig. 2.

IV. CONCLUSION

Analysis of recent high-performance implosions at the NIF has demonstrated the propagation of the burn wave into the cold fuel layer, this being an essential aspect in achieving ignition [22–25]. Electrothermal filamentation within the shell may have a variety of important implications for the resulting burn dynamics within the dense fuel. Stratification in the cold electron temperature is rapidly translated into the ion temperature by collisions over the shell equilibrium time $\tau^{\mathrm{eq}} \sim 0.1$ ps. Temperature structures larger than a few μm may self-heat through alpha emission due to the strong locality of alpha heating in the shell [26], leading to "runaway" hot regions in the fuel. The self-generated magnetic field associated with the ETI may also be relevant; It is well established that burn propagation is inhibited by a perpendicular magnetic field [27,28]. Unlike studies considering magnetization associated with Rayleigh-Taylor spikes on the inner cold fuel surface [29,30], magnetic field growth due to ETI filamentation will arise even in effectively spherical implosions, and may suppress burn propagation into the shell.

ACKNOWLEDGMENTS

This work was supported by the UKRI-STFC Grant No. ST/V001655/1. The authors gratefully acknowledge the support of the ARCHER2 support team, the UKRI-EPSRC/IBM Computational Discovery program, members of the Norreys research group at the University of Oxford, and useful conversations with Dr. A. Bott and Prof. A. R. Bell.

[1] M. G. Haines, Thermal instability and magnetic field generated by large heat flow in a plasma, especially under laser-fusion conditions, Phys. Rev. Lett. **47**, 917 (1981).
[2] R. W. Paddock, H. Martin, R. T. Ruskov, R. H. H. Scott, W. Garbett, B. M. Haines, A. B. Zylstra, R. Aboushelbaya, M. W. Mayr, B. T. Spiers, R. H. W. Wang, and P. A. Norreys, One-dimensional hydrodynamic simulations of low convergence ratio direct-drive inertial confinement fusion implosions, Phil. Trans. R. Soc. A **379**, 20200224 (2021).
[3] K. J. Peterson, D. B. Sinars, E. P. Yu, M. C. Herrmann, M. E. Cuneo, S. A. Slutz, I. C. Smith, B. W. Atherton, M. D. Knudson, and C. Nakhleh, Electrothermal instability growth in magnetically driven pulsed power liners, Phys. Plasmas **19**, 092701 (2012).
[4] S. A. Slutz, M. C. Herrmann, R. A. Vesey, A. B. Sefkow, D. B. Sinars, D. C. Rovang, K. J. Peterson, and M. E. Cuneo, Pulsed-power-driven cylindrical liner implosions of laser preheated fuel magnetized with an axial field, Phys. Plasmas **17**, 056303 (2010).
[5] O. Willi and P. T. Rumsby, Filamentation on laser irradiated spherical targets, Opt. Commun. **37**, 45 (1981).
[6] O. Willi, P. T. Rumsby, C. Hooker, A. Raven, and Z. Q. Lin, Observations of instabilities in the corona of laser produced plasmas, Opt. Commun. **41**, 110 (1982).
[7] G. Thiell and B. Meyer, Thermal instabilities as an explanation of jet-like structures observed on laser irradiated thin planar targets at 1.06 μm and 0.35 μm wavelengths, Laser Part. Beams **3**, 51 (1985).
[8] L. J. Dhareshwar, P. A. Naik, P. D. Nandwana, and H. C. Pant, Characteristics of plasma flow from laser irradiated planar thin foil targets, J. Appl. Phys. **61**, 4458 (1987).
[9] T. A. Hall and L. M. Newell, Ultra-short pulse filamentation in a laser-produced plasma, Opt. Commun. **70**, 213 (1989).
[10] S. D. Baton, C. Labaune, G. Mathieussent, and W. Seka, Study of Schlieren diagnostics to investigate filamentation in plasmas with long density scale lengths, Opt. Commun. **70**, 50 (1989).
[11] J. R. Rygg, F. H. Séguin, C. K. Li, J. A. Frenje, M. J.-E. Manuel, R. D. Petrasso, R. Betti, J. A. Delettrez, O. V. Gotchev, J. P. Knauer, D. D. Meyerhofer, F. J. Marshall, C. Stoeckl, and W. Theobald, Proton radiography of inertial fusion implosions, Science **319**, 1223 (2008).
[12] E. M. Epperlein and A. R. Bell, Non-local analysis of the collisional Weibel instability in planar laser-ablated targets, Plasma Phys. Control. Fusion **29**, 85 (1987).
[13] T. Mochizuki, T. Yabe, K. Mima, K. Yoshikawa, H. Azechi, A. Kikuchi, and C. Yamanaka, Ablation nonuniformity on laser irradiated pellet and collisional hot electron filamentation, Jpn. J. Appl. Phys. **19**, L645 (1980).
[14] D. A. Tidman and R. A. Shanny, Field-generating thermal instability in laser-heated plasmas, Phys. Fluids **17**, 1207 (1974).
[15] W. Rozmus, A. V. Brantov, M. Sherlock, and V. Y. Bychenkov, Return current instability driven by a temperature gradient in ICF plasmas, Plasma Phys. Control. Fusion **60**, 014004 (2018).
[16] S. I. Braginskii, Transport processes in a plasma, Rev. Plasma Phys. **1**, 205 (1965).
[17] Critical parameters of metals, in *Physics of Strongly Coupled Plasma*, edited by V. Fortov, I. Iakubov, and A. Khrapak (Oxford University Press, Oxford, 2006).
[18] Y. T. Lee and R. M. More, An electron conductivity model for dense plasmas, Phys. Fluids **27**, 1273 (1984).
[19] F. Lambert, V. Recoules, A. Decoster, J. Clérouin, and M. Desjarlais, On the transport coefficients of hydrogen in the inertial confinement fusion regime, Phys. Plasmas **18**, 056306 (2011).
[20] J. Derouillat, A. Beck, F. Pérez, T. Vinci, M. Chiaramello, A. Grassi, M. Flé, G. Bouchard, I. Plotnikov, N. Aunai, J. Dargent, C. Riconda, and M. Grech, SMILEI: A collaborative, open-source, multi-purpose particle-in-cell code for plasma simulation, Comput. Phys. Commun. **222**, 351 (2018).
[21] F. Pérez, L. Gremillet, A. Decoster, M. Drouin, and E. Lefebvre, Improved modeling of relativistic collisions and collisional ionization in particle-in-cell codes, Phys. Plasmas **19**, 083104 (2012).
[22] A. L. Kritcher, A. B. Zylstra, D. A. Callahan, O. A. Hurricane, C. R. Weber, D. S. Clark, C. V. Young, J. E. Ralph, D. T. Casey, A. Pak *et al.*, Design of an inertial fusion experiment exceeding the Lawson criterion for ignition, Phys. Rev. E **106**, 025201 (2022).
[23] H. Abu-Shawareb *et al.* (Indirect Drive ICF Collaboration), Lawson criterion for ignition exceeded in an inertial fusion experiment, Phys. Rev. Lett. **129**, 075001 (2022).
[24] A. B. Zylstra, A. L. Kritcher, O. A. Hurricane, D. A. Callahan, J. E. Ralph, D. T. Casey, A. Pak, O. L. Landen, B. Bachmann, K. L. Baker *et. al.*, Experimental achievement and signatures

of ignition at the National Ignition Facility, Phys. Rev. E **106**, 025202 (2022).

[25] H. Abu-Shawareb *et al.* (Indirect Drive ICF Collaboration), Achievement of target gain larger than unity in an inertial fusion experiment, Phys. Rev. Lett. **132**, 065102 (2024).

[26] C. Lin, B. He, Y. Wu, and J. Wang, Energy deposition and deflection of α particles in hot dense plasmas relevant to inertial confinement fusions, Nucl. Fusion **63**, 076018 (2023).

[27] B. Appelbe, A. L. Velikovich, M. Sherlock, C. Walsh, A. Crilly, S. O' Neill, and J. Chittenden, Magnetic field transport in propagating thermonuclear burn, Phys. Plasmas **28**, 032705 (2021).

[28] R. D. Jones and W. C. Mead, The physics of burn in magnetized deuterium-tritium plasmas: spherical geometry, Nucl. Fusion **26**, 127 (1986).

[29] C. A. Walsh, J. P. Chittenden, K. McGlinchey, N. P. L. Niasse, and B. D. Appelbe, Self-generated magnetic fields in the stagnation phase of indirect-drive implosions on the national ignition facility, Phys. Rev. Lett. **118**, 155001 (2017).

[30] C. A. Walsh and D. S. Clark, Biermann battery magnetic fields in ICF capsules: Total magnetic flux generation, Phys. Plasmas **28**, 092705 (2021).